IEEE Photonics Journal
An IEEE Photonics Society Publication

Open Access

Impact of Thermal-Induced Turbulent Distribution Along FSO Link on Transmission of Photonically Generated mmW Signals in the Frequency Range 26–40 GHz

Volume 12, Number 1, February 2020

Luis Vallejo
Matej Komanec
Beatriz Ortega, *Member, IEEE*
Jan Bohata
Dong-Nhat Nguyen, *Member, IEEE*
Stanislav Zvanovec, *Senior Member, IEEE*
Vicenç Almenar, *Member, IEEE*

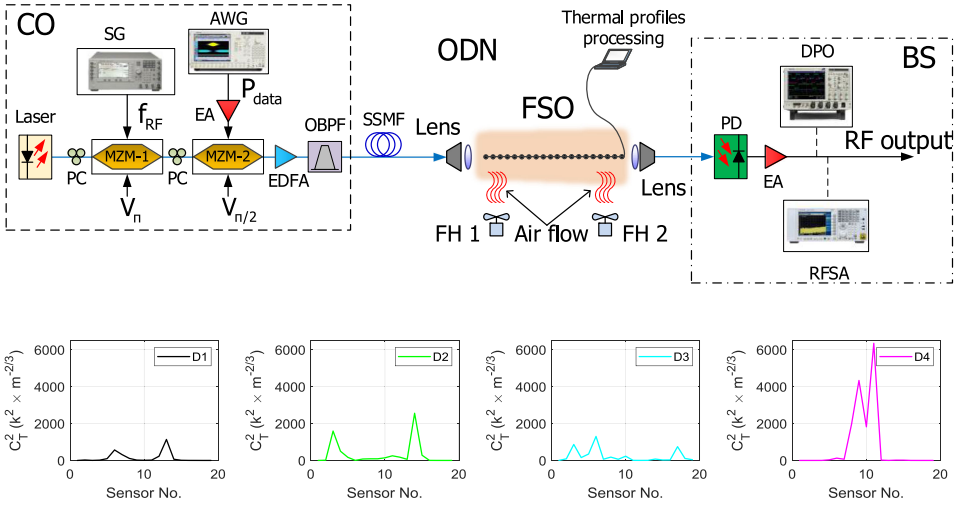

DOI: 10.1109/JPHOT.2019.2959227

Impact of Thermal-Induced Turbulent Distribution Along FSO Link on Transmission of Photonically Generated mmW Signals in the Frequency Range 26–40 GHz

Luis Vallejo [1], **Matej Komanec** [2], **Beatriz Ortega** [1], ***Member, IEEE***, **Jan Bohata** [2], **Dong-Nhat Nguyen** [2], ***Member, IEEE***, **Stanislav Zvanovec** [2], ***Senior Member, IEEE***, **and Vicenç Almenar** [1], ***Member, IEEE***

[1]Instituto de Telecomunicaciones y Aplicaciones Multimedia, Universitat Politecnica de Valencia, Camino de vera, 46022 Valencia, Spain
[2]Department of Electromagnetic Field, Faculty of Electrical Engineering, Czech Technical University in Prague, 166 27 Prague, Czech Republic

DOI:10.1109/JPHOT.2019.2959227

Manuscript received November 5, 2019; revised December 4, 2019; accepted December 7, 2019. Date of publication December 11, 2019; date of current version January 17, 2020. This work was supported in part by the Research Excellence Award Programme GVA under Grant PROMETEO 2017/103 and in part by the Spanish Ministerio de Ciencia, Innovación y Universidades, under RTI2018-101658-B-I00 FOCAL Project and MEYS Project LTC18008 within COST CA16220. Corresponding author: Luis Vallejo (e-mail: luivalc2@iteam.upv.es).

Abstract: Microwave photonics is a promising solution to transmit millimeter wave (mmW) signals for the 5th generation (5G) mobile communications as part of a centralized radio access network (C-RAN). In this paper, we experimentally evaluate the impact of turbulent free space optics links on photonically generated mmW signals in the frequency range of 26−40 GHz. We analyze the remote generation of mmW signals over hybrid links based on free-space optics (FSO) and standard single mode optical fiber (SSMF) with −39.97 dBm received electrical power and phase noise level at 100 kHz as low as −95.92 dBc Hz at 26 GHz. Different thermal distributions along the FSO link have been implemented and Gamma-Gamma model has been employed to estimate the thermally induced turbulence. The results show high electrical power decrease and fluctuation of the generated mmW signal according to the particular level of the turbulence in terms of refractive index structure parameter and thermal distribution along the FSO link. 8 Gb/s 16-quadrature amplitude modulation (QAM) data transmission at 42 GHz has been demonstrated over the hybrid link with minimal error vector magnitude (EVM) value of 5% whereas turbulent FSO link introduced up to 5 dB power penalty.

Index Terms: Access networks, free space optics, millimeter waves, microwave photonics.

1. Introduction

Mobile data traffic is expected to grow up to 77 exabytes per month by 2022 according to [1], i.e., a sevenfold increase over 2017, which leads to a compound annual growth rate of 46% from 2017

to 2022. To deal with such explosive growth, the 3rd Generation Partnership Project (3GPP) has been developing the new upcoming mobile network, known as the 5th generation (5G). However, 5G will not only be an evolution of the mobile network but represent significant progress in wireless communications since it requires massive machine-type communications, ultra-reliable and low latency communications, enhanced mobile broadband and ultra-fast data transfer [2] to support emergency services and applications such as internet of things, mobile ultra-high definition video streaming or autonomous driving [3].

5G definition includes the proposal of two main frequency bands: FR1 (below 6 GHz) and FR2 (24.25−52.60 GHz) [4]. Nowadays, the spectrum below 6 GHz is congested due to many current wireless services. However, millimeter-wave (mmW) technology, in which frequency range can exceed 100 GHz, will play a key role in 5G networks due to its enormous available bandwidth [5]. In this context, radio over fiber (RoF), basically consisting of an optical carrier modulated by a radio signal, is a promising technology for cloud radio access networks (C-RAN) [6]. In such architecture, optical distribution networks (ODN) deliver mmW signals from a central office (CO) over variable long distances to many remote base stations (BS) with low attenuation, immunity to radio frequency interference, transparency to modulation formats, high capacity, flexibility and dynamic resource allocation as its main advantages [7].

Microwave photonics, as a discipline combining microwave and photonic fields, has been recently extensively employed to generate mmW signals with low phase noise and frequency tenability [8]. The simplest method to photonically generate high radio frequency signal is to beat two heterodyne lasers separated by the desired frequency, but phase control loop or optical injection locking techniques are required for frequency and phase stabilization [9]. The literature shows various proposals to generate mmW signals by using multimode light sources, such as dual-mode lasers, mode-locked lasers, Fabry-Perot lasers or supercontinuum sources but in general, these designs need to be customized and they are therefore costly [10]. Moreover, optical fiber non-linear effects such as four-wave mixing [11], cross-gain modulation [12] or stimulated Brillouin Scattering [13] have also been proposed for mmW signal generation schemes with even more increased cost and complexity.

The use of external modulation by a $LiNbO_3$ Mach-Zehnder modulator (MZM) shows an excellent compromise among the aforementioned factors. A continuous optical wave (CW) is modulated by a radio signal, and optical frequency multiplication is achieved when two sidebands, separated by the desired frequency, beat each other at the photodetector [14]. Frequency doubling, quadrupling and up to octupling [15] have been recently demonstrated allowing to reduce the electric bandwidth requirements significantly.

The transmission of radio signals over free-space optics (FSO), so-called RoFSO [16], offers typical flexibility of wireless communications and speed of light transmission [17]. It also provides a higher level of coverage and mobility while exploiting unlicensed frequencies in the optical wireless domain [18]. Furthermore, the FSO link can be employed to transmit multiple wavelength division multiplexed (WDM) channels simultaneously. Nevertheless, FSO is highly affected by atmospheric phenomena, especially by thermal turbulence. The thermal distribution can vary significantly based on the day time and as well within the urban environment due to several sources of heating [19], [20]. High thermal differences can be experienced, e.g., up 30 $^{\circ}$C [19], resulting in different turbulence levels in the vicinity of buildings, air conditions, highways, masts and in and over the street canyons – see illustrated temperature profile across a city in Fig. 1.

In this paper, mmW signals in the frequency range of 26−40 GHz are photonically generated by using a MZM biased at the carrier suppression point. Furthermore, 8 Gb/s signal transmission is demonstrated over 40 GHz mmW signal along the RoF/FSO link and system penalties have been measured under different thermal-induced turbulence distributions along the FSO channel. To the best authors' knowledge, this paper presents for the first time the experimental characterization of mmW signals transmission at such a frequency band under turbulence on RoF/FSO links providing an estimation of the impact of different temperature distributions.

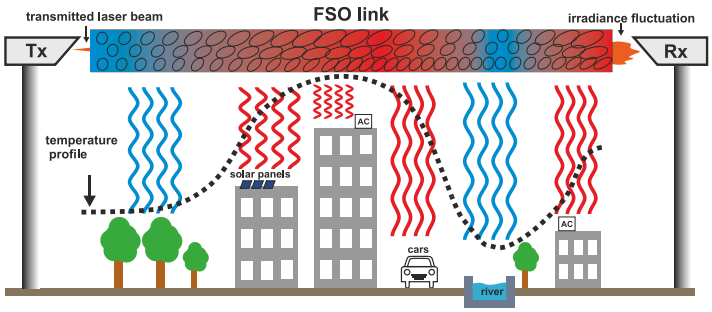

Fig. 1. Illustration of different turbulent flows influencing FSO in urban areas.

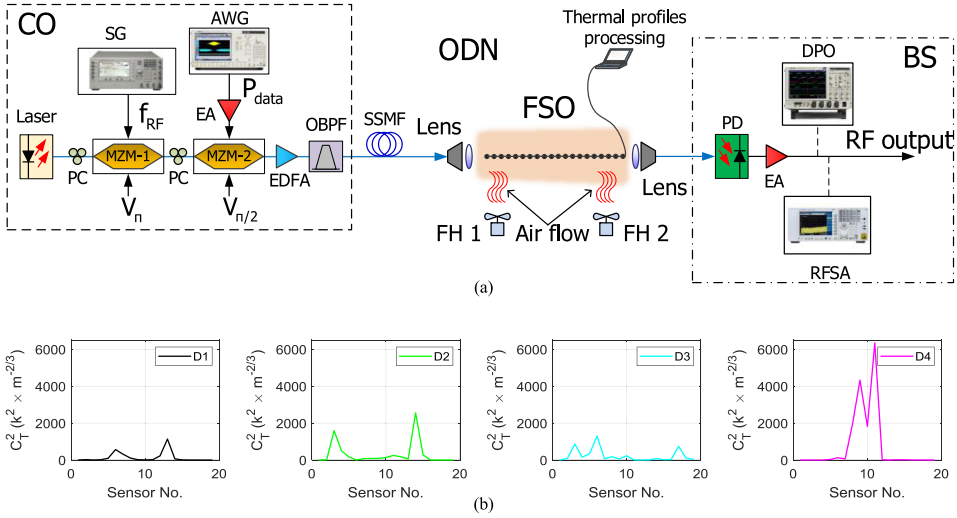

Fig. 2. (a) Experimental setup (CO: central office, ODN: optical distribution network, PC: polarization controller, MZM: Mach–Zehnder modulator, AWG: arbitrary waveform generator, EA: electrical amplifier, EDFA: erbium-doped fiber amplifier, OBPF: optical bandpass filter, SSMF: standard single mode fiber, FSO: free-space optics, FH: fan heater, PD: photodetector, RFSA: RF spectrum analyzer, DPO: digital phosphor oscilloscope), and (b) C_T^2 distributions.

2. System Description

The experimental setup of mmW signal transmission over a hybrid optical link of SSMF and FSO is shown in Fig. 2(a). A distributed feedback (DFB) laser (EXFO IQS) at a wavelength of 1550.12 nm with an output optical power of 10 dBm provides the optical carrier. A polarization controller (PC) adjusts the state of polarization to minimize MZM-1 (Photline MX-LN-40) losses. MZM-1 is biased at null transmission point (half-wave voltage, V_π), i.e., at 6.4 V, to obtain the carrier suppressed double sideband (CS-DSB) modulated signal. The optical carrier is then modulated by a radio frequency (RF), f_{RF}, which is generated by a signal generator (Agilent PSG E8267C) with an output RF power of 22 dBm.

The experimental setup employs another PC before a second modulator, MZM-2 (Avanex PowerBit F-10), which is biased at the linear point (quadrature voltage $V_{\pi/2}$), i.e., 5.8 V. The optical signal is then modulated by the data generated by an arbitrary waveform generator (AWG, Tektronix AWG7122C). Note that the data signal with 28 dBm output power is amplified by a 12 dB gain RF electrical amplifier (Minicircuits ZX60-14012L-S+).

The modulated optical signal is amplified by an erbium-doped fiber amplifier (EDFA, Amonics EDFA-23-B-FA) with 13 dBm output power and filtered out by an optical bandpass filter (OBPF,

Finisar Waveshaper 4000S) having a bandwidth of $\Delta\lambda = 1.5$ nm to reduce amplified spontaneous emission. The signal is then launched into 1.4 km long standard single mode fiber (SSMF) what is followed by a 1.2 m long FSO channel using a pair of air-spaced doublet collimators (Thorlabs F810APC-1550). The FSO link loss is 4.5 dB, which is significantly lower compared to free space propagation of radio waves in the mmW band.

Artificial turbulence is produced on the FSO channel according to four different spatial temperature distributions (D1–D4), as shown in Fig. 2(b). The distribution is expressed in terms of the temperature structure parameter C_T^2 distribution along the link, which is explained further. Turbulence is generated by two fan heaters introducing temperature gradients into the FSO channel and measured by 20 temperature sensors equidistantly located along the FSO link with 0.06 m spacing. These distributions represent inhomogeneous temperature profile when the collimated laser beam propagates in FSO link through differently heated areas, according to Fig. 1. D1 introduces almost uniform turbulence along the link, whereas in the case of D2 and D3, the fans' thermal flow was set in order to reach increased thermal gradient close to the receiver and transmitter, respectively, which can be induced e.g., by thermal flow close to the building/masts of transmitting/receiving FSO heads. Finally, D4 represents peak turbulence in the middle of the link, which can be caused e.g., by an increased airflow over the street canyons, roads or air-condition outlets as indicated in Fig. 1.

According to photonic mmW signal generation approach based on external CS-DSB modulated signals [14], the mmW signal $f_{\mathrm{mmW}} = 2f_{RF}$, is generated after beating the modulated sidebands at photodetector (PD, Finisar BPDV2020R) and subsequently, it is amplified by an RF electrical amplifier (SHF-810). The mmW signal is analyzed by an RF spectrum analyzer (RFSA) showing the RF signal potentially launched to an antenna located in the C-RAN BS infrastructure.

3. Turbulence Effect on FSO System

FSO is widely affected by atmospheric phenomena including high attenuation due to fog, rain, snow or irradiance fluctuation, known as scintillation, as a result of the optical turbulence [21]. The extent of field amplitude fluctuation in the atmospheric turbulence can be characterized by the log-amplitude variance σ_R^2, commonly referred to as Rytov parameter, which is related to the refractive index structure parameter C_n^2 for a plane wave as follows [22]:

$$\sigma_R^2 = 2.25k^{7/6} \int_0^L C_n^2(x)\,(L-x)^{5/6} dx, \tag{1}$$

where k is the wave number and L is the horizontal distance travelled by the optical field/radiation. Note that, uniform C_n^2 leads to Rytov variance given by:

$$\sigma_R^2 = 1.23k^{\frac{7}{6}} C_n^2 L^{\frac{11}{6}}, \tag{2}$$

The C_n^2 parameter, which determines the strength of the turbulence, is defined as:

$$C_n^2 = \left(79 \times 10^{-6} \frac{P_a}{T^2}\right)^2 C_T^2, \tag{3}$$

where P_a is the atmospheric pressure in millibars and C_T^2 is the temperature structure parameter, which is defined as:

$$C_T^2 = (T_1 - T_2)^2 / L_p^{2/3}. \tag{4}$$

T_1 and T_2 are temperatures at two points separated by distance L_p. Therefore, based on the thermal distributions along the FSO propagation path, it is possible to determine C_T^2 and consequently C_n^2. According to the Gamma-Gamma (GG) atmospheric turbulence (AT) model [23], the probability

TABLE 1
Refractive Index and Temperature Structure Parameters of Different Temperature Distributions

Turbulent scenarios	C_T^2 $(K^2\, m^{-2/3})$	C_n^2 $(m^{-2/3})$ (L=1.2 m)	C_n^2 $(m^{-2/3})$ (L=500 m)
D1	138.01	$1 \cdot 10^{-10}$	$1.6 \cdot 10^{-15}$
D2	315.59	$2.3 \cdot 10^{-10}$	$3.6 \cdot 10^{-15}$
D3	227.83	$1.5 \cdot 10^{-10}$	$2.4 \cdot 10^{-15}$
D4	775.43	$5.7 \cdot 10^{-10}$	$8.9 \cdot 10^{-15}$

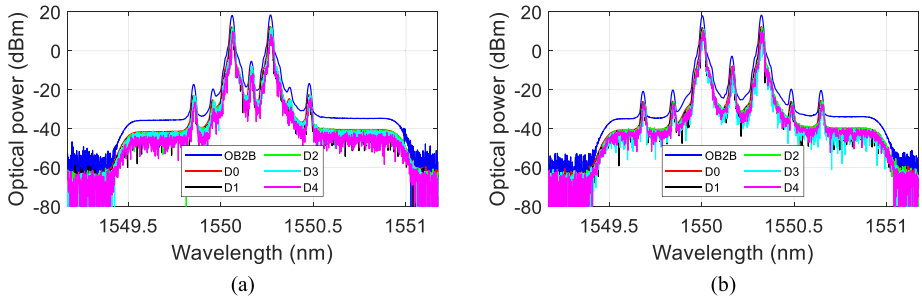

Fig. 3. Optical spectra of the carrier-suppressed RF modulated signal (Resolution bandwidth (RBW) = 0.02 nm) for different turbulence conditions at different frequencies: (a) 26 GHz and (b) 40 GHz.

of a given intensity I at the end of the link is given by:

$$P(I) = \frac{2(\alpha\beta)^{(\alpha+\beta)/2}}{\Gamma(\alpha)\Gamma(\beta)} I^{(\alpha+\beta)/2-1} K_{\alpha-\beta}\left(2\sqrt{\alpha\beta I}\right)$$

$$\alpha = \exp\left[\frac{0.49\sigma_R^2}{\left(1+1.11\sigma_R^{\frac{12}{5}}\right)^{\frac{5}{6}}}\right] - 1, \quad \beta = \exp\left[\frac{0.51\sigma_R^2}{\left(1+0.69\sigma_R^{\frac{12}{5}}\right)^{\frac{5}{6}}}\right] - 1 \tag{5}$$

where $1/\alpha$ and $1/\beta$ are the variances of the small and large scale eddies, respectively, $\Gamma(\cdot)$ is the Gamma function and $K_{\alpha-\beta}(\cdot)$ is the modified Bessel function of the second kind. The intensity fluctuations are characterized by the probability distribution, which is classified as: Weak turbulence ($\sigma_R^2 < 1$), Moderate turbulence ($\sigma_R^2 \approx 1$)or Strong turbulence ($\sigma_R^2 > 1$).

In our setup, turbulence is generated using two fans blowing hot air perpendicular into the FSO channel in order to create a thermal gradient along the optical propagation path. Table 1 shows the averaged C_T^2 and C_n^2 corresponding to D1–D4 temperature distributions in our experiment. Note that the spacing between adjacent sensors is $L_p = 0.06$ m, the atmospheric pressure $P_a = 1024$ mm and wavelength $\lambda = 1550.12$ nm. Direct calculation of Rytov variance ($\sigma_R^2 < 0.05$ in all cases) leads to a weak turbulence regime in our experimental setup. In order to show impact for a longer span, C_n^2 values have been recalculated via σ_R^2 to reflect 500 m FSO transmission distance.

The effect of the turbulence on the optical signal transmitted over the FSO channel is shown by the optical spectra comparison of the OB2B and the hybrid links (D0–D4) under different turbulent levels in Fig. 3(a) and (b) for 26 GHz and 40 GHz, respectively. Note that optical power measurements over FSO link employ higher sensitivity mode in the optical spectrum analyzer, leading to lower noise level. The turbulent-induced signal fluctuations in the optical domain result in reduced optical power by values up to 3 dB and 4 dB for the highest impact turbulence distributions at 26GHz and 40 GHz, respectively, with respect to D0.

Fig. 4(a) shows the RF spectra of the signal generated at 26 GHz after opto-electronic conversion and measured by the MXA analyzer (Agilent N9020A) in order to evaluate the impact of the

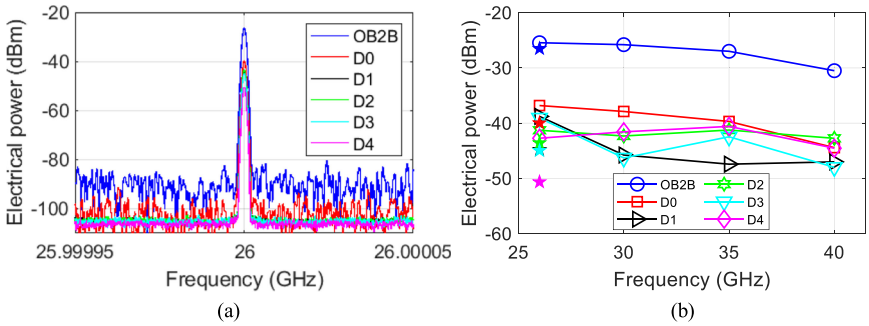

Fig. 4. Impact of turbulence on the electrical power: (a) Spectral distribution and (b) Dependence on the electrical frequency.

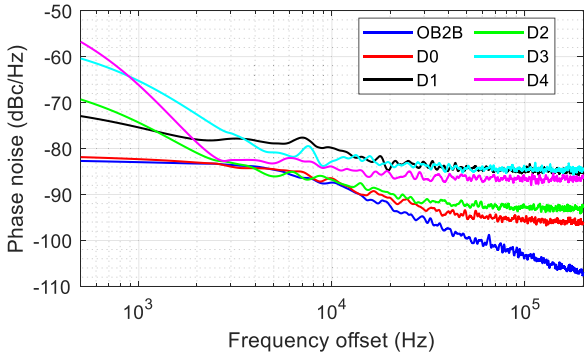

Fig. 5 Phase noise measurements at 26 GHz (RBW = 220 Hz).

turbulence along the FSO transmission in terms of RF power and also the noise floor. The measured received electrical power for OB2B is −26.5 dBm, whereas −39.97 dBm is obtained after transmission over the hybrid link without induced turbulence (D0) and up to 12 dB power decrease is measured when turbulence (D1–D4) is applied in the FSO link. Note that trace average mode is employed to reduce the noise level after FSO transmission in the RFSA. Nevertheless, no effects on the signal linewidth can be observed.

Fig. 4(b) shows the measured electrical power of the signal in the frequency range of 26−40 GHz mmW after photodiode by using PNA-X (Agilent N4373C). Star markers at 26 GHz show the results obtained by the high-resolution MXA analyzer where each color represents different temperature distribution according to D1–D4 profiles. As expected, the RF power decreases due to the overall system frequency response when the frequency increases, as shown in the OB2B and D0 curves over 26−40 GHz, with a total drop of 7.7 dB. However, this value is not constant for measurements under thermally induced turbulence due to power fluctuations. The power drop about 2 dB is measured for D2 and D4, whereas values over 8 dB are obtained for D1 and D3.

Fig. 5 depicts the phase noise measured at 26 GHz by MXA for different temperature distributions and Table 2 summarizes phase noise results at different offsets. The phase noise at 100 kHz offset is measured as −103.36 dBc/Hz for OB2B, whereas it is increased up to −95.92 dBc/Hz for D0 with a further increase under the turbulent regimes. As observed in Fig. 5, the impact of D1–D4 turbulence results in a higher phase noise level due to both power decrease and increased noise floor. Whereas scenario D2 with increased turbulence level close to the receiver shows the lowest phase noise among D1–D4 at 100 kHz, the highest phase noise is induced by scenarios D1 and D3 where the turbulence level is uniformly distributed and increased close to the transmitter, respectively.

TABLE 2
Phase Noise Measurements in dBc/Hz of 26 GHz Generated Signal at Different Offsets (RBW = 220 Hz)

		Frequency offset		
		$1\ kHz$	$10\ kHz$	$100\ kHz$
Scenario	OB2B	-82.97	-87.41	-103.36
	D0	-82.32	-86.49	-95.92
	D1	-75.42	-79.85	-84.85
	D2	-74.36	-86.80	-92.77
	D3	-65.29	-82.81	-84.34
	D4	-66.2	-83.93	-86.75

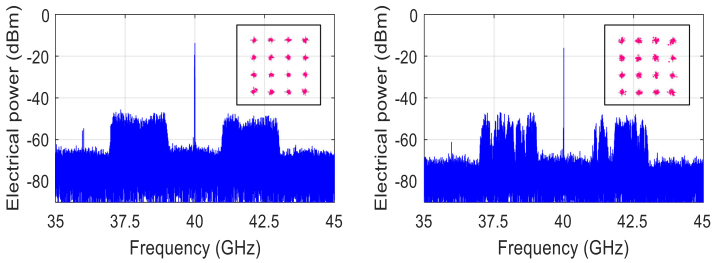

Fig. 6. Electrical spectrum of 8 Gb/s 16-QAM data signal over 40 GHz with 1 dBm at the receiver input for: (a) D0, and (b) under D3 turbulence profile. Insets show the corresponding constellation diagrams.

4. Data Transmission Experiment

In this section, an RF carrier at 20 GHz is employed to generate a 40 GHz mmW signal, which is further modulated by 16-QAM signal with 2 GHz bandwidth. Note that the modulating signal, using pseudorandom binary sequence (PRBS) length of 2^9-1, has a center frequency of 2 GHz. It results in a bitrate of 8 Gb/s throughout the hybrid ODN.

Fig. 6 shows the electrical spectra for 40 GHz mmW signals carrying 8 Gb/s data when the received optical power at PD input is 1 dBm. The RF carrier and data power is -16 dBm and -53 dBm, respectively, after transmission over the hybrid link without induced turbulence, i.e., scenario D0, which is shown in Fig. 6(a). Note that an RF electrical post-detection amplifier with 29 dB gain is employed before the signal analyzer. Fig. 6(b) shows the impact of the D3 turbulence profile on the transmitted spectrum where data signal bands undergo a time-varying fading effect due to interference between signals with different random delays at the receiver. Insets in Fig. 6(a) and (b) show the received 16-QAM constellation, whose error vector magnitudes (EVMs) are 5.1% and 6%, respectively. Note that, the EVM is measured by a digital phosphor oscilloscope (DPO) (Tektronix DPO72004C).

Finally, Fig. 7 plots the obtained EVM versus the received optical power at PD input for all tested scenarios. Since only 1.4 km SSMF and 1.2 m long FSO channel are employed, there is no significant power penalty between OB2B and D0. The EVM values of OB2B and D0 are kept below the limit of 12.5% for optical power up to -4.3 dBm at the optical receiver whereas minimum EVM of 5% is measured for a received power of 1 dBm. The largest EVM impact of turbulence has been obtained under D1 temperature distribution which represents evenly distributed turbulence along the channel. The power penalty is in this case almost 5 dB at 12.5% of EVM, compared to D0. The EVM can be kept below 12.5% for received optical power up to -2.1 dBm for D2, D3 and D4 when turbulence highly influences the areas closer to the receiver and transmitter or exhibit a peak in the center of the link, respectively. However, at least 0.3 dBm of received optical power is required

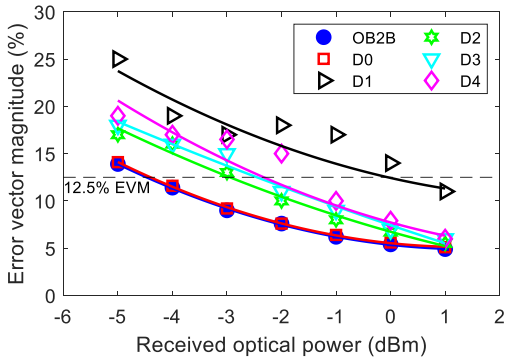

Fig. 7. Measured error vector magnitude (EVM) for different links and temperature distributions for 8 Gb/s 16-QAM signal over 40 GHz mmW signal.

for D1. Note that, despite the high phase noise level and low electrical power measurements in this scenario, the conducted measurements showed that evenly distributed turbulence in the FSO link has the highest impact on EVM performance in such system and the distribution of scintillations along the link also plays a key role in the signal transmission penalty.

5. Conclusions

In this paper, for the first time, we have experimentally demonstrated the impact of different turbulent distributions along the RoFSO link on mmW signal transmissions in the frequency range of 26−40 GHz in a hybrid FSO/SSMF network. Optical carrier suppression at MZM has been used to generate double frequency signals, i.e., the measured RF power and phase noise at 100 kHz offset at 26 GHz were −39.97 dBm and −95.92 dBc/Hz, respectively. Moreover, 8 Gb/s 16-QAM data signal transmission at 42 GHz has been demonstrated over hybrid links with an EVM as low as 5% providing enough capacity for considered transmission within 5G networks. Several turbulence distributions along the FSO link have been implemented and their impact on the signal transmission have been evaluated. We experimentally verified that the highest impact on RoFSO link transmission can be expected under turbulence evenly distributed along the link. The measured turbulence scenarios resulted in up to 5 dB power penalty in terms of received optical power for EVM level of 12.5% in comparison with the performance of the hybrid link without turbulence.

References

[1] "Cisco visual networking index: Forecast and trends, 2017-2022," Cisco, Feb. 2019. [Online]. Available: https://www.cisco.com/c/en/us/solutions/collateral/service-provider/visual-networking-index-vni/white-paper-c11-741490.pdf
[2] 3GPP, "5G; Study on scenarios and requirements," 3GPP, Sophia Antipolis Cedex, France, Tech. Rep. 38.913 V 15.0.0, 2018.
[3] R. Waterhouse and D. Novack, "Realizing 5G: Microwave photonics for 5G mobile wireless systems," *IEEE Microw. Mag.*, vol. 16, no. 8, pp. 84–92, Sep. 2015.
[4] 3GPP, "5G; NR; User Equipment (UE) radio transmission and reception; Part 2: Range 2 Standalone," 3GPP, Sophia Antipolis Cedex, France, TS 38.101-2 V 15.5.0, 2019.
[5] X. Wang *et al.*, "Millimeter wave communication: A comprehensive survey," *IEEE Commun. Surveys Tuts.*, vol. 20, no. 3, pp. 1616–1653, Jul.–Sep. 2018.
[6] A. Checko *et al.*, "Cloud RAN for mobile networks - A technology overview," *IEEE Commun. Surveys Tuts.*, vol. 17, no. 1, pp. 405–426, Jan.–Mar. 2015.
[7] C. H. Lee, *Microwave Photonic*, 2nd ed. Boca Raton, FL, USA: CRC Press, 2013.
[8] J. Yao, "Microwave photonics," *J. Lightw. Technol.*, vol. 27, no. 3, pp. 314–335, Feb. 2009.
[9] Y. Doi, S. Fukushima, T. Ohno, and K. Yoshino, "Frequency stabilization of millimeter-wave subcarrier using laser heterodyne source and optical delay line," *IEEE Photon. Technol. Lett.*, vol. 13, no. 9, pp. 1002–1004, Sep. 2001.
[10] J. Liu *et al.*, "Efficient optical millimeter-wave generation using a frequency-tripling Fabry–Pérot laser with sideband injection and synchronization," *IEEE Photon. Technol. Lett.*, vol. 23, no. 18, pp. 1325–1327, Sep. 2011.

[11] L. Xu, C. Li, S. M. G. Lo, and H. K. Tsang, "Millimeter wave generation using four wave mixing in silicon waveguide," *OECC 2010 Tech. Dig.*, Jul. 2010, pp. 860–861.
[12] Y.-K. Seo, C.-S. Choi, and W.-Y. Choi, "All-optical signal up-conversion for radio-on-fiber applications using cross-gain modulation in semiconductor optical amplifiers," *IEEE Photon. Technol. Lett.*, vol. 14, no. 10, pp. 1448–1450, Oct. 2002.
[13] T. Kanesa *et al.*, "Dual pump brillouin laser for RoF millimeterwave carrier generation with tunable resolution," in *Proc. IEEE Region 10 Conf.*, Nov. 2015, pp. 1–6.
[14] G. Qi, J. Yao, J. Seregelyi, S. Paquet, and C. Belisle, "Generation and distribution of a wide-band continuously tunable millimeter-wave signal with an optical external modulation technique," *IEEE Trans. Microw. Theory Techn.*, vol. 53, no. 10, pp. 3090–3097, Oct. 2005.
[15] H. Zhang, C. Lin, S. Xie, K. Zhang, X. Wu, and Z. Dong, "A novel radio-over-fiber system based on carrier suppressed frequency eightfold millimeter wave generation," *IEEE Photon. J.*, vol. 9, no. 5, pp. 1–6, Oct. 2017, Art no. 7203506.
[16] J. Bohata, M. Komanec, J. Spáčil, Z. Ghassemlooy, S. Zvánovec, and R. Slavík, "24-26 GHz radio over fiber and free space optics for 5G systems," *Opt. Lett.*, vol. 43, no. 5, pp. 1035–1038, Mar. 2018.
[17] J. Bohata, S. Zvanovec, P. Pesek, T. Korinek, M. Mansour Abadi, and Z. Ghassemlooy, "Experimental verification of long-term evolution radio transmissions over dual-polarization combined fiber and free-space optics optical infrastructures," *Appl. Opt.*, vol. 55, no. 8, pp. 2109–2116, Mar. 2016.
[18] J. Bohata, M. Komanec, J. Spáčil, S. Zvánovec, Z. Ghassemlooy and R. Slavík, "Hybrid RoF-RoFSO system using directly modulated laser for 24–26 GHz 5G networks," in *Proc. 11th Int. Symp. Commun. Syst. Netw. Digit. Signal Process.*, 2018, pp. 1–5.
[19] J. Libich and S. Zvanovec, "Influences of turbulences in near vicinity of buildings on free-space optical links," *IET Microw. Antennas Propag.*, vol. 5, no. 9, pp. 1039–1044, 2011.
[20] K. Niachou, I. Livada, and M. Santamouris, "Experimental study of temperature and airflow distribution inside an urban street canyon during hot summer weather conditions—Part I: Air and surface temperatures," *Build. Environ.*, vol. 43, no. 8, pp. 1383–1392, Aug. 2008.
[21] S. Bloom, E. Korevaar, J. Schuster, and H. Willebrand, "Understanding the performance of free-space optics [Invited]," *J. Opt. Netw.*, vol. 2, no. 6, pp. 178–200, May 2003.
[22] L. C. Andrews and R. L. Phillips, *Laser Beam Propagation Through Random Media*, 2nd ed. Bellingham, WA, USA: SPIE Press, 2005.
[23] M. A. Khalighi and M. Uysal, "Survey on free space optical communication: a communication theory perspective," *IEEE Commun. Surveys Tuts.*, vol. 16, no. 4, pp. 2231–2258, Oct.–Dec. 2014.